ACS OMEGA

http://pubs.acs.org/journal/acsodf
Article

Hagenia abyssinica-Biomediated Synthesis of a Magnetic Fe_3O_4/NiO Nanoadsorbent for Adsorption of Lead from Wastewater

Published as part of ACS Omega virtual special issue "Magnetic Nanohybrids for Environmental Applications".

Abdurohman Eshetu Ferenj, Daniel Manaye Kabtamu, Ayalew H. Assen, Gangaraju Gedda, Adem Ali Muhabie, Mhamed Berrada, and Wubshet Mekonnen Girma*

Cite This: *ACS Omega* 2024, 9, 6803−6814

ABSTRACT: Magnetic nanocomposite adsorbents are cost-effective, environmentally friendly, easy to use, and highly efficient at removing metals from large volumes of wastewater in a short time by using an external magnetic field. In this study, an Fe_3O_4/NiO composite nanoadsorbent was prepared by varying the mass percent ratios of NiO (50, 40, 30, 20%), which are denoted Fe_3O_4/50%NiO, Fe_3O_4/40%NiO, Fe_3O_4/30%NiO, and Fe_3O_4/20%NiO, respectively, using *Hagenia abyssinica* plant extract as the template/capping agent and a simple mechanical grinding technique. The nanocomposites were characterized using an X-ray diffractometer (XRD), scanning electron microscopy (SEM), Fourier transform infrared (FT-IR) spectroscopy, nitrogen adsorption, and ζ-potential measurements. The adsorption performance of the nanoadsorbent was assessed for the removal of lead (Pb^{2+}) ions from aqueous solutions. Among the composite adsorbents, Fe_3O_4/50%NiO demonstrated the best Pb(II) removal efficiency (96.65%) from aqueous solutions within 80 min at pH 8, at a 100 mg/L lead concentration and 0.09 g of adsorbent dose. However, with the same parameter, only 62.8% of Pb(II) was removed using Fe_3O_4 nanoparticles (NPs). The adsorptive performance indicated that the optimum amount of porous material (NiO) in the preparation of the Fe_3O_4/NiO composite nanoadsorbent, with the aid of *H. abyssinica* plant extract, enhances the removal of toxic heavy metals from aqueous solutions. Multiple isotherm and kinetic models were used to analyze the equilibrium data. Adsorption isotherm and kinetic studies were found to follow the Freundlich isotherm and pseudo-second-order kinetics, respectively.

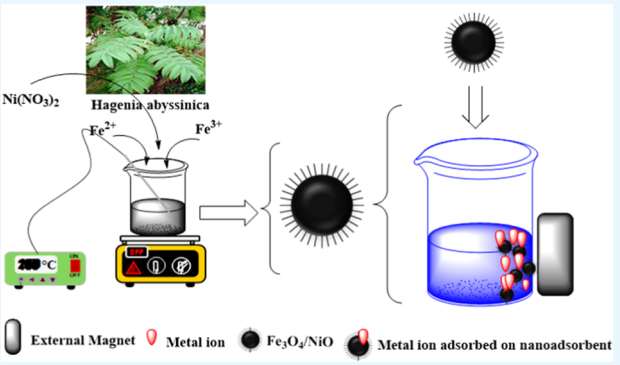

1. INTRODUCTION

One of the most urgent environmental issues is the contamination of ecosystems by heavy metals including Pb^{2+}. Industry and other human activities can release toxic, nonbiodegradable heavy metals into water bodies, threatening the ecological system and public health, resulting in various diseases and disorders.[1] It is easy for heavy metals to be conjugated with small metabolites, nucleic acids, and proteins, in living things, which can alter or eliminate biological function and/or disrupt the organism's metal control site.[2] Thus, research into heavy metal removal from aqueous solutions is of significant interest.

Several physicochemical techniques, including solvent extraction,[3] chemical precipitation,[4] membrane separation, adsorption, and ion exchange,[5,6] can be used to remove heavy metals from polluted water. Nevertheless, these techniques have limitations, such as a lack of complete treatment, the need for costly equipment, extensive labor and close monitoring, chemical reagents, and the production of large quantities of either solid waste or sludge that must be disposed of in addition to the original waste.[7,8] Furthermore, because these methods do not apply to large volumes, they have not successfully met water resource demand.[9] One of the highly effective and straightforward strategies for eliminating heavy metal ions is adsorption technology, which is dependent on cutting-edge adsorbent materials.[10] For heavy metal removal, various adsorbents were used, including activated carbons,[11] carbon nanotubes,[12] and natural inorganic mineral-functionalized polymers and porous materials.[13−16] The main drawback of all of the previous adsorbents was that they were difficult to separate and regenerate from wastewater. Consequently, novel adsorbents with remarkable adsorption

Received: October 17, 2023
Revised: January 9, 2024
Accepted: January 16, 2024
Published: February 2, 2024

https://doi.org/10.1021/acsomega.3c08151
ACS Omega 2024, 9, 6803−6814

ability and facile separation of heavy metals from a large quantity of water remain in demand.

Magnetic nanocomposite adsorbents remove heavy metals from aqueous solutions.[17,18] They are the most effective wastewater remediation methods because they are economical, easy to use, eco-friendly, and fast in removing heavy metal ions from large volumes of wastewater using an external magnetic field. In this regard, the use of iron-based magnetic nanoadsorbents, the pure form of magnetite nanoparticles (NPs) (Fe_3O_4) as an example, has received a great deal of attention. The main drawback of pure Fe_3O_4 NPs is their lower surface area, limiting their adsorption capacity and responses to an external magnetic field and the consequential recovery of the adsorbents after treatment.[19,20] Modification of the surface effects of Fe_3O_4 by combining them with other high-surface-area materials has been considered to be a sound strategy to circumvent the drawback. For example, Yan et al.[21] synthesized iron oxide/manganese dioxide/graphene-based magnetic nanocomposites for separation of hexavalent chromium and reported that the nanocomposite was stable and easily recovered due to its magnetic nature. Similarly, magnetic sorbents including Fe_2O_3@C core−shell NPs,[22] iron−carbon nanocomposites,[23] magnetic floating foams,[24] porous charcoal/iron oxide nanocomposites derived from a metal−organic framework,[25] magnetic exfoliated graphite,[26] epoxidized natural rubber-magnetite nanocomposites,[27] polystyrene-iron oxide nanocomposites,[28] zerovalent Fe loaded onto expanded graphite, and activated carbon FeO composite[29] are used to remove the contaminants via magnetic separation. This work is then aimed at preparing an iron oxide-based nanocomposite adsorbent that combines the magnetic property of iron oxide and the high surface area of NiO.

The preparation method of nanoadsorbents is another important factor to consider. A simple and environmentally benign procedure that leads to a controllable particle size is needed. For this reason, nanocomposite adsorbents synthesized using renewable biological sources as a template are green and environmentally friendly for wastewater treatment. Because of the presence of various phenolic groups, plant leaf extracts can be used as stabilizing and reducing agents in synthesizing metal NPs. These phytochemicals act as a reducing agent, converting the metal salt to its atomic metal state, and as a capping agent, stabilizing the particles in the dispersing medium and preventing agglomeration during the synthesis process. Furthermore, biomediated NP synthesis is advantageous because it does not require expensive chemicals, reduces the use of toxic chemicals, and can be processed at low energy levels.[30] Among the natural biological resources, *Hagenia abyssinica* is a medicinal plant that could potentially be used as a template for the synthesis of nanocomposite adsorbents in wastewater treatment. It is selected for the green synthesis of nanocomposites as it contains many potentially active phytochemicals that play an essential role in the reduction or stability of NPs during the synthesis process.[31] Because of the presence of biomolecules such as saponins, phlobathanins, flavonoids, anthraquinones, phenols, terpenoids, alkaloids, steroids, glycosides, and tannins[32] in *H. abyssinica* that are potential reducing or capping agents, plant extract was used as a templating/capping agent for preventing aggregation, controlling particle size, and biofunctionalization during synthesis. The various functional groups present in the plant could act as reducing/capping agents and stabilize the nanoparticles during the assembly process. The use of plant extracts to assist the formation of Fe_3O_4 nanoparticles has been demonstrated in the literature.[33] In comparison to NPs derived from other additives, those derived from plants and their extracts have been shown to have a faster synthesis process, greater stability, better-regulated form and size, and higher levels of important reducing agents.[34]

Herein, we report the first-time use of *H. abyssinica*-biomediated synthesis of the Fe_3O_4/NiO nanocomposite for the adsorption and removal of heavy metals from contaminated water. The current work is, to the best of our knowledge, the first attempt to explore the synthesis of Fe_3O_4/NiO using a natural product as a reducing agent from metal salts to their respective metal oxides. Furthermore, the prepared nanoadsorbent was characterized by using various techniques and tested for the selected heavy metal adsorption.

2. MATERIALS AND METHODS

2.1. Chemicals and Reagents. Ferrous sulfate heptahydrate ($FeSO_4{\cdot}7H_2O$, 99.5%), ferric chloride ($FeCl_3$, 99%), sodium hydroxide (NaOH, 99.8%), nickel nitrate hexahydrate ($Ni(NO_3)_2{\cdot}6H_2O$, 98%), ammonia (NH_3, 25%), nickel chloride hexahydrate ($NiCl_2{\cdot}6H_2O$, 97%), sodium bicarbonate ($NaHCO_3$, 99%), ethanol (CH_3CH_2OH, 99.9%), hydrochloric acid (HCl, 37%), and deionized water (DI) were used during the experiments. All reagents used are of an analytical-grade quality and were used without any additional purification.

2.2. Preparation of *H. abyssinica* Plant Extract. Fresh, matured, and green *H. abyssinica* leaves were collected from the Wollo University Dessie campus and washed with running tap water and deionized water (DI) to remove dust particles. The clean leaves were then dried at room temperature in the absence of light before being ground with an electric grinder. 20 g of powder was placed in an Erlenmeyer flask with 500 mL of distilled water. Afterward, the mixture was shaken for 30 min with a mechanical shaker. Then, the solution was kept at 50 °C for 1 h under a magnetic stirrer and cooled to room temperature. Next, the obtained solution was filtered through Whitman No.1 filter paper to get a clear solution. Finally, the filtrate was reflexed at 110 °C for 6 h, centrifuged at 5000 rpm for 30 min, and stored at 4 °C for further use.

2.3. *H. abyssinica* Plant Extract-Mediated Synthesis of Magnetite (Fe_3O_4) NPs. $FeSO_4{\cdot}7H_2O$ (0.1 M) and $FeCl_3$ (0.05 M) solutions were dissolved in 100 mL of DI water and vigorously stirred for 5 min. The solutions were then added, drop by drop, to a beaker containing 20 mL of *H. abyssinica* plant extract. Subsequently, the solution was stirred, and 80 mL of (1 M NaOH) was added slowly. The solution's color immediately changed from orange to dark-brown color, representing the formation of Fe_3O_4 NPs. The solution was cooled to room temperature. Magnetic separation was used to collect the precipitate, which was purified with deionized water. The black products were oven-dried for 24 h at 80 °C.

2.4. *H. abyssinica* Plant Extract-Mediated Synthesis of NiO NPs. A 2.0 M aq. solution of NH_4OH was slowly added into a 0.50 M aq. solution of $Ni(NO_3)_2{\cdot}6H_2O$ under magnetic stirring. Then, the mixture was kept at 80 °C until it turned dark blue, signifying the development of the $[Ni(NH_3)_6]^{2+}$ complex. Simultaneously, 50 mL of plant extract was gradually added while stirring for 90 min. The solution turned into a light-green color. The obtained solution was filtered, and the precipitate was purified with deionized water and ethanol. Next, the compound was dried in an oven at 100 °C for 12 h. The grayish-black-colored NiO NPs were attained by calcining

https://doi.org/10.1021/acsomega.3c08151
ACS Omega 2024, 9, 6803−6814

Scheme 1. Schematic Representations of *H. abyssinica* Plant Extract-Mediated Synthesis of Fe_3O_4/NiO Nanocomposites[a]

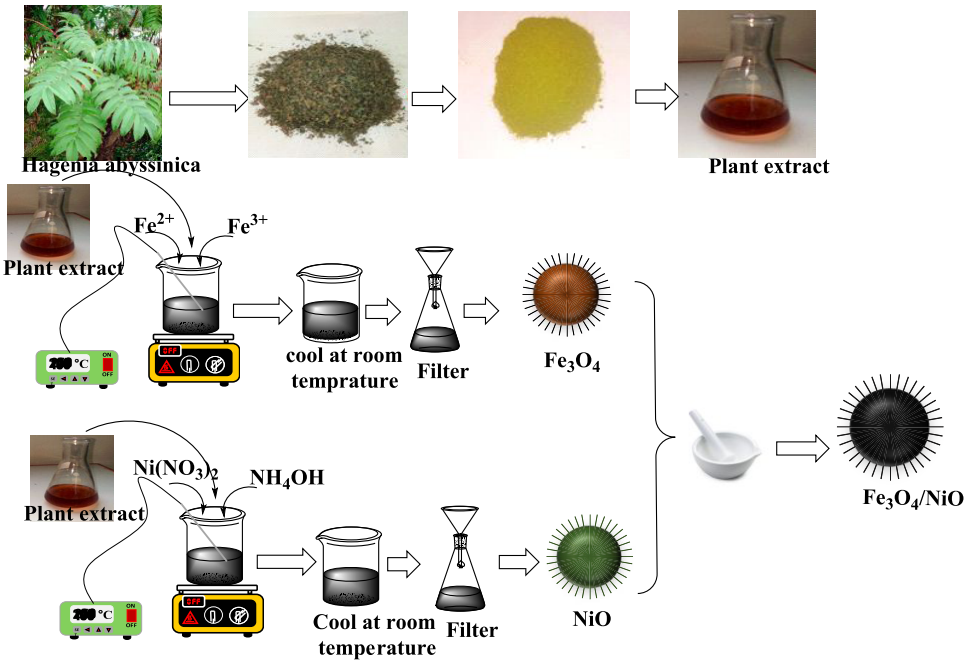

[a]Photos in figures were taken by A.E.F., and the scheme was developed by W.M.G.

$Ni(OH)_2$ powder in a furnace for 2 h at a temperature of 300 °C.

2.5. *H. abyssinica* Plant Extract-Mediated Synthesis of Fe_3O_4/NiO Nanocomposites. The plant extract-mediated Fe_3O_4/NiO nanoadsorbent synthesis was accomplished with a simple approach. In this experiment, nanocomposites were formed by combining different mass ratios of Fe_3O_4 and NiO NPs by altering the mass ratios of NiO (50, 40, 30, and 20%). The various ratios were thoroughly mixed before being calcined at 300 °C for 2 h.

2.6. Batch Adsorption Experiments. Experiments with batch adsorption were performed to determine the adsorption capacities of Fe_3O_4/NiO nanocomposites for the elimination of Pb(II) ions from wastewater. The adsorption experiment was also performed for Fe_2O_3 NPs with the same parameter as a control. A synthetic lead solution was mixed with 60−140 mg/L adsorbent (Fe_3O_4/NiO nanocomposites), stirred for 4 h, and then left for 24 h to reach equilibrium before being filtered. The optimal amount of the adsorbent was determined by plotting the percentage of removal against the mass of the adsorbent. The influence of contact time was tested in the range of 20−100 min, and the pH range was studied in the range of 2−10. Afterward, the concentration of the metal in the filtrate was estimated by using atomic absorption spectroscopy (AAS). The following equations were utilized to determine the adsorption capacity as well as the removal efficiency.

$$Q_e = \frac{(C_0 - C_e)}{W} \times V \quad (1)$$

$$R\,\% = \frac{(C_0 - C_e)}{C_0} \times 100 \quad (2)$$

Here, Q_e is the concentration of Pb^{2+} ions adsorbed on the nanocomposite at equilibrium, R is percentage removal, V is the volume of the metal ion solution in L, W is the weight of the adsorbent, i.e., nanocomposite in gram scale, and C_0 and C_e are the initial and equilibrium concentrations (in mg/L), respectively.

2.7. Recovery Studies. For desorption studies, metal-adsorbed NPs were first washed with ultrapure water to remove the unadsorbed metals loosely attached to the vial and adsorbent. Pb ion can be desorbed by using HCl, and different concentrations of HCl eluent varying from 0.001 to 0.2 M were used for desorption experiments. To study recovery, Fe_3O_4/NiO regeneration and metal readsorption were carried out in three consecutive cycles. For each cycle, 0.09 g of Fe_3O_4/50%NiO nanoadsorbent was mixed with 60 mL of 100 mg/L of each metal solution in a glass vial. After each adsorption−desorption cycle, the Fe_3O_4/50%NiO nanoadsorbent was washed thoroughly with ultrapure water to neutrality and reconditioned for adsorption in the succeeding cycle. Once equilibrium was reached, the nanoadsorbent was separated with a magnet, and the supernatant was kept to measure the concentration of Pb using AAS, and all experiments were performed in triplicate.

2.8. Characterization. X-ray diffraction (XRD) was executed using a Shimadzu XRD-7000. The size and surface morphology of the nanocomposite were obtained by field-emission scanning electron microscopy (FESEM, JSM 6500F, JEOL). Fourier transform infrared (FT-IR) spectra were attained by using 65 FT-IR (PerkinElmer) spectroscopy. Nitrogen adsorption measurements were carried out on the 3-Flex Surface Characterization Analyzer (Micromeritics) with guest-free (evacuated) samples at pressures of up to 1 bar. The surface areas were estimated using the Brunauer−Emmett−Teller (BET) model from nitrogen adsorption isotherms collected at 77 K. Pore size distribution was analyzed using a BJH model from the desorption branch. The DW-AA320N Atomic Absorption spectrometer (AAS) was used for adsorption studies.

ζ-Potential measurements were conducted using the Zetasizer Pro BLUE equipment from Malvern, U.K. The

https://doi.org/10.1021/acsomega.3c08151
ACS Omega 2024, 9, 6803−6814

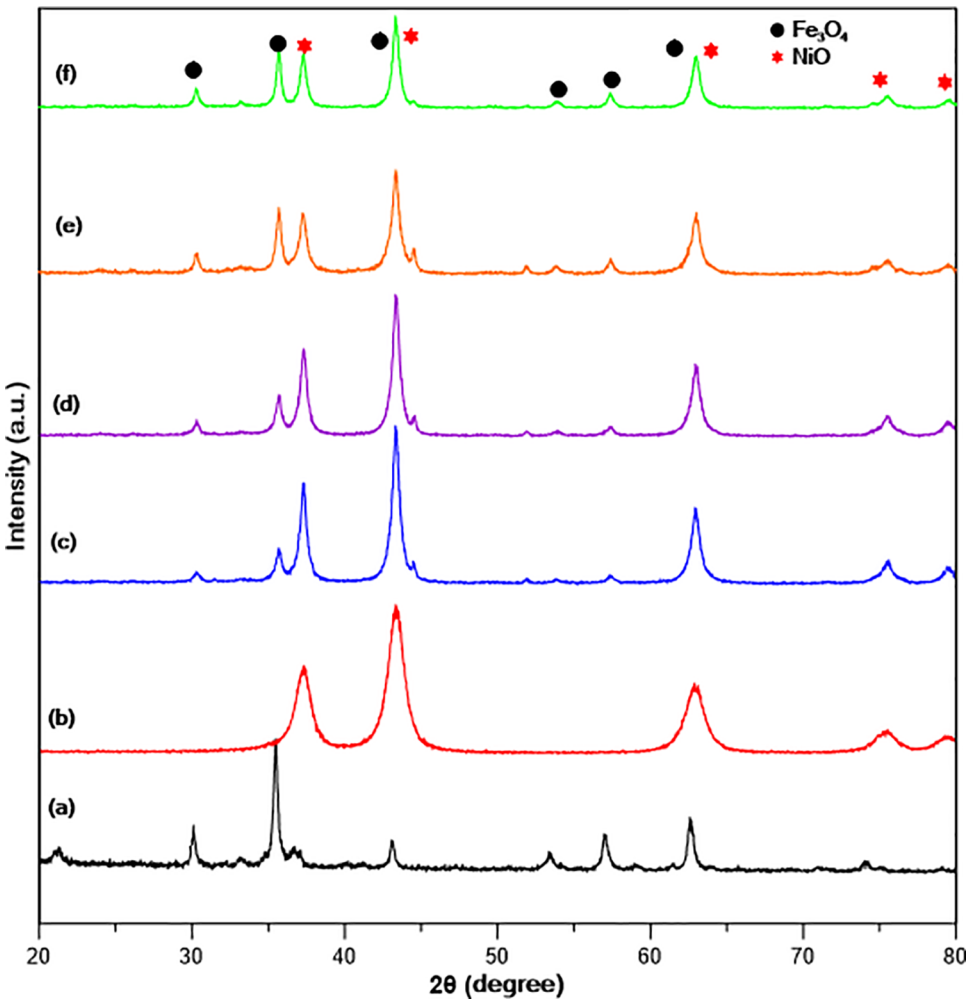

Figure 1. XRD patterns for (a) Fe_3O_4, (b) NiO, and (c) 50:50%, (d) 60:40%, (e) 70:30% and (f) 80:20% of Fe_3O_4/NiO.

electrophoretic mobility of particles was automatically calculated and then converted to ζ-potential using the Smoluchowski equation (eq 3).

$$\zeta = (\eta \times \mu)/\varepsilon \tag{3}$$

Here, ζ represents the ζ-potential, η is the dynamic viscosity of the fluid, μ is the particle mobility, and ε is the dielectric constant. For the preparation process, 0.1 g of nanoadsorbent was conditioned in 100 mL of deionized water under stirring for 15 min, resulting in a 0.1% solid ratio. The solution pH was adjusted using 0.1 mol/L HCl and 0.1 mol/L NaOH. Afterward, the solution was left undisturbed for 30 min to let the larger particles settle.

3. RESULTS AND DISCUSSION

3.1. Synthesis and Characterization. As demonstrated in Scheme 1, the nanocomposite preparation was conducted by synthesizing each nanoparticle (NP) from the corresponding salt precursors. Fe_3O_4 NPs were synthesized from Fe^{2+} and Fe^{3+} salt by using the co-precipitation method. Under continuous stirring, *H. abyssinica* leaf extract was slowly added to the solution. Afterward, the pH of the solution was adjusted by adding NaOH, and the color changed to dark brown. In the same protocol, NiO NPs were fabricated using $Ni(NO_3)_2{\cdot}6H_2O$ and NH_4OH, and a grayish-black product was obtained. Finally, fine powders of Fe_3O_4 and NiO were mixed with appropriate ratios and crushed with a mortar and pestle; the resulting nanocomposite was calcined using a muffle furnace, and finally, the Fe_3O_4/NiO nanocomposite was obtained.

The phase and structure of the prepared nanoadsorbent were checked by XRD. Figure 1a–f indicates the XRD patterns of Fe_3O_4, NiO, and Fe_3O_4/NiO, which were synthesized in the presence of *H. abyssinica* extracts with different molar ratios of iron and nickel. The (220), (311), (222), (400), (511), and (440) planes show magnetite (Fe_3O_4) with corresponding major diffraction peaks at 30.12, 35.48, 43.10, 53.41, 57.01, and 62.60°, respectively (JCPDS No. 19-0629). Furthermore, the XRD peaks of NiO with (111), (200), (220), (311), and (222) planes at 37.28, 43.35, 62.86, 75.31, and 79.33° confirm the phase purity of the synthesized NP (JCPDS No. 47-1049). As displayed in the XRD patterns, a decrease in the percentage of NiO and clearly visible Fe_3O_4 peaks were noticed for the composites. The results demonstrate that the Fe_3O_4/NiO nanocomposite was successfully synthesized.

The surface morphologies of the synthesized nanoparticles were analyzed using a scanning electron microscope (SEM). Figure 2a–c shows the SEM images of Fe_3O_4, NiO, and Fe_3O_4/NiO. Figure 2d depicts the corresponding EDS of the Fe_3O_4/NiO nanocomposite. Fe_3O_4 particles have different shapes, with spherical microstructures being the dominant ones, shown in Figure 2a. There is also some degree of

https://doi.org/10.1021/acsomega.3c08151
ACS Omega 2024, 9, 6803−6814

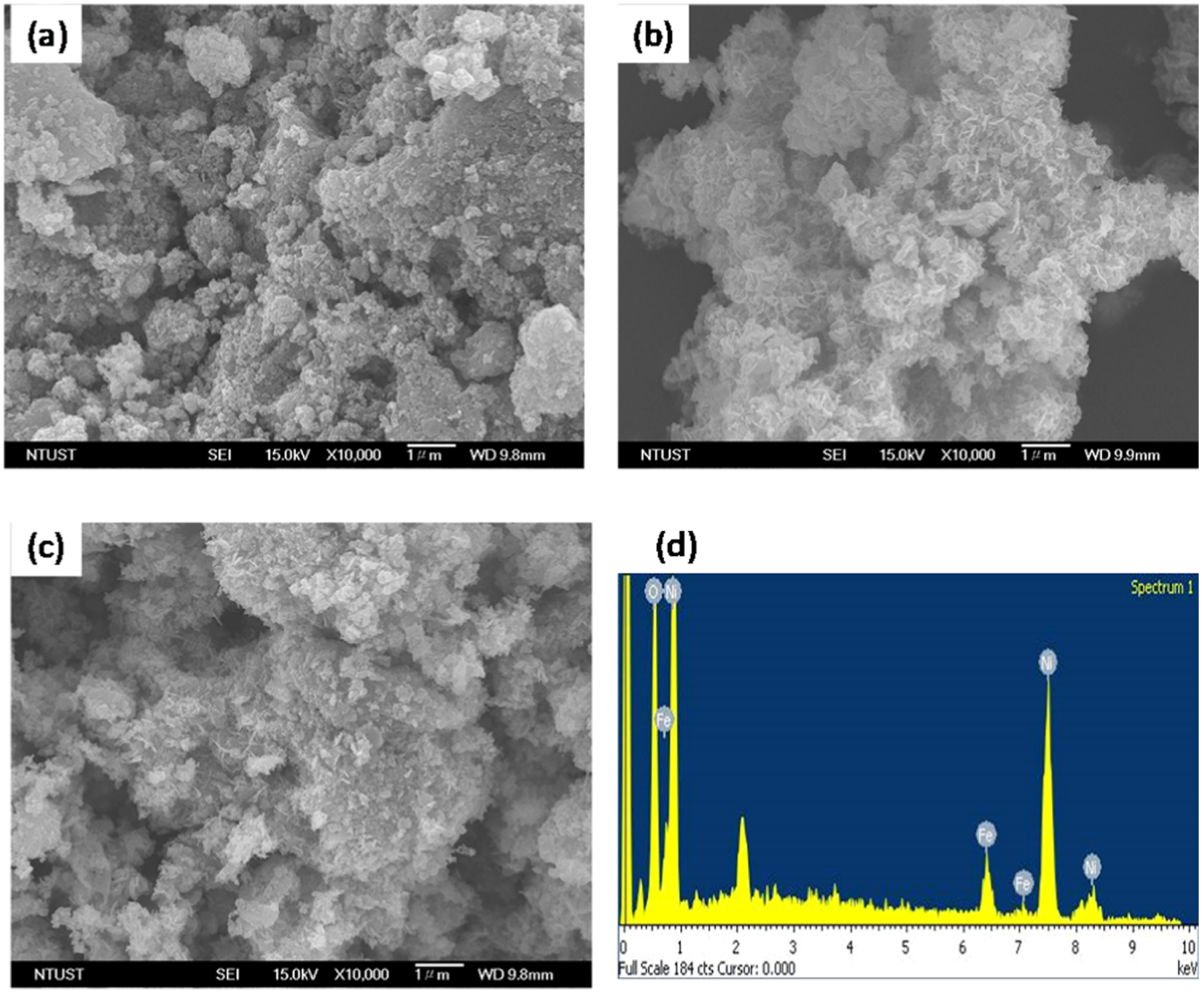

Figure 2. SEM images for (a) Fe_3O_4, (b) NiO, (c) 50% Fe_3O_4/NiO, and (d) SEM EDS 50% Fe_3O_4/NiO.

agglomeration with very finely interconnected particles. Figure 1b depicts the micrographs of pure NiO with a nanosheet-type morphology. SEM micrograph of the Fe_3O_4/NiO nanocomposite, shown in Figure 1c, reveals the coexistence of microstructures from both phases, i.e., the agglomerated particles of the Fe_3O_4 phase and the nanosheets of the NiO phase. This confirms the formation of the nanocomposite. The EDS analysis, carried out to study the elemental composition of the prepared nanocomposite, confirmed the presence of Fe, Ni, and O atoms in the Fe_3O_4/NiO sample. The result further substantiates the successful formation of the Fe_3O_4/NiO nanoadsorbent.

FT-IR characterization was also performed to further support the formation of the nanocomposite. As shown in Figure 3, the FT-IR spectra show a broad peak ranging from 3700 to 3300 cm^{-1}, attributable to the stretching vibrations of −OH groups. The characteristic bands at about 2900, 1700, and 1050 cm^{-1} can be ascribed to the stretching vibrations of the −CH, −COOH, and C−O groups of the plant extract, respectively,[33] which confirms the possible presence of hydroxy and carboxylic functional groups in the extract. The peaks around 970 cm^{-1} are ascribed to OH out-of-plane bands.[35]

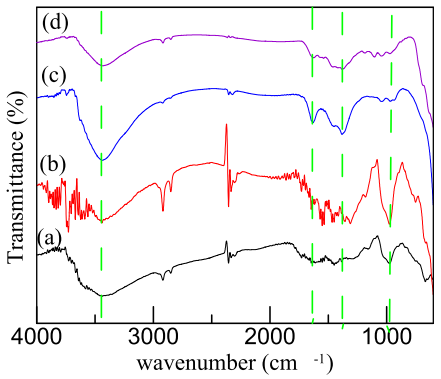

Figure 3. FT-IR spectra of (a) *H. abyssinica* plant extract, (b) Fe_3O_4, (c) NiO, and (d) Fe_3O_4/NiO.

The peak around 600 cm^{-1} can be ascribed to the Fe−O stretching peak.[36]

After confirming the phase purity and functional groups of the samples, the N_2 adsorption experiment measured at 77 K was used to deduce the surface area and porosity of the synthesized NPs. Prior to the N_2 adsorption tests, about 200

https://doi.org/10.1021/acsomega.3c08151
ACS Omega 2024, 9, 6803−6814

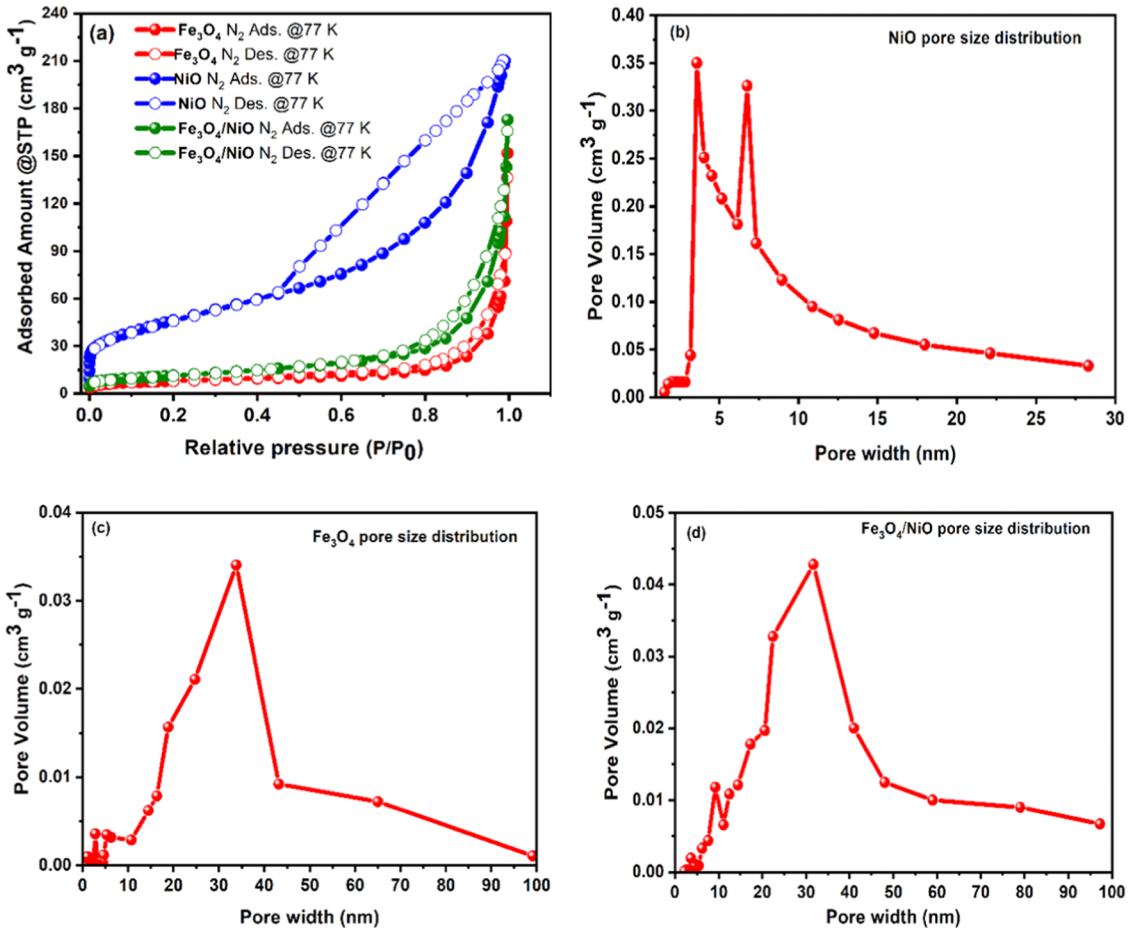

Figure 4. Nitrogen adsorption−desorption isotherms for Fe_3O_4, NiO, and 50% Fe_3O_4/NiO nanoadsorbents (a) and the corresponding pore size distribution analysis of NiO (b), Fe_3O_4 (c), and 50% Fe_3O_4/NiO (d).

mg of the as-synthesized materials was evacuated/activated by heating the samples under a dynamic vacuum at 150 °C for 8 h. The nitrogen adsorption isotherms recorded at 77 K (Figure 4a) showed that the pure NiO NP exhibited a type-IV isotherm, a characteristic of a mesoporous material according to the International Union of Pure and Applied Chemistry (IUPAC) classification, with BET surface areas of about 150 m^2 g^{-1}. Pure Fe_3O_4 and 50% Fe_3O_4/NiO nanoadsorbents possess type V isotherm shapes with small hysteresis at high relative pressures. This property is also a characteristic of mesoporous adsorbents with weak adsorbate−adsorbent interactions at low relative pressures. The pore size distributions of the nanoadsorbents, deduced from the corresponding N_2 isotherms applying the BJH desorption model, evidenced the presence of mesopores (Figure 4b−d). As expected, the incorporation of the more porous NiO within Fe_3O_4 resulted in the looked-for enhancement of the BET surface area and porosity of the composite adsorbent while retaining the magnetic property of magnetite, with the nanocomposite exhibiting a higher surface area (38 m^2 g^{-1}) than the pure Fe_3O_4 NP (26 m^2 g^{-1}).

3.2. Adsorption Studies. *3.2.1. Effect of pH.* The initial pH of the metal ion solution plays a significant role in monitoring the adsorption process. The initial pH was optimized in the range 2−10 with an interaction time of 80 min and a Pb(II) ion concentration of 60 mg/L and Fe_3O_4/50%NiO dose of 0.03 g at 25 °C under an agitation speed of 200 rpm. As displayed in Figure 5a,b, both adsorption capacity and percent removal of lead enhanced as the pH increased from pH 2 to 8 using both Fe_3O_4 and Fe_3O_4/NiO nanocomposites. The repulsive forces between the predominant positively charged protonic species of the nanoadsorbent surfaces and Pb^{2+} ions decrease the adsorption of lead ions. However, at moderate pH, linked protons are released from the adsorbent surface and might increase the adsorption of Pb on the nanocomposite. A higher pH aqueous solution promotes surface deprotonation of the nanoadsorbents, which increases the attractive forces between the more negatively charged adsorbent surface and the Pb(II) ions and, hence, the adsorption capacity (Figure 5b). However, a sharp decrease in adsorption of Pb(II) at pH values of 8−10 might be caused by the presence of insufficient Pb(II) ions to be adsorbed due to the precipitation of lead hydroxide, $Pb(OH)_2$, in the high-pH water sample.[37] The maximum percent removal values for Fe_3O_4 and Fe_3O_4/NiO were 82.98 and 85.97%, respectively, at pH 8 (Figure 5b). The removal of Pb at lower pH is smaller, possibly due to protons occupying the adsorption sites. Therefore, the optimum pH value was decided to be 8.

To delve further into the nanoadsorbent−heavy metal interaction, we measured the ζ-potential of the nanoadsorbents across varying pH values. As depicted in Figure 6, the surface charge for both Fe_3O_4 and the Fe_3O4/NiO nanocomposite exhibited an increasingly negative trend with rising pH, thereby enhancing electrostatic interactions and contributing to higher metal adsorption. At lower pH levels, deprotonation of

https://doi.org/10.1021/acsomega.3c08151
ACS Omega 2024, 9, 6803−6814

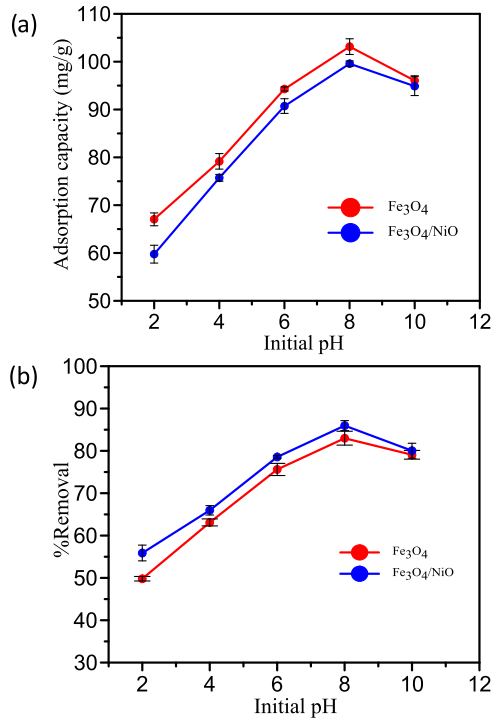

Figure 5. Effect of initial pH on the (a) adsorption capacity of Pb and (b) removal efficiency of Pb by Fe_3O_4 and 50% Fe_3O_4/NiO nanocomposite.

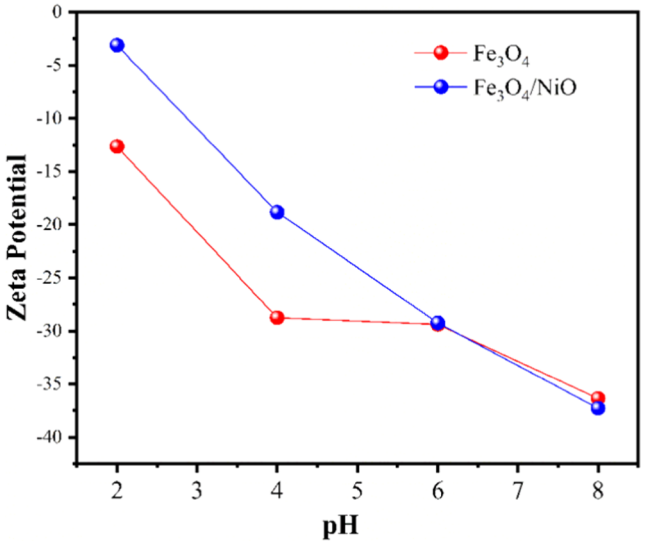

Figure 6. ζ-Potential vs pH of Fe_3O_4 and Fe3O4/NiO nanocomposite adsorbents.

functional groups (possibly −OH and −COOH) is limited. However, as the pH levels increased, the excess of hydroxide ions (OH^-) expedited the deprotonation process, resulting in a shift toward a negative surface charge. Notably, the Fe_3O_4/NiO nanocomposite demonstrated more pronounced deprotonation compared to Fe_3O_4, leading to its substantially higher negative surface charge (−37 mV) at elevated pH levels (≈8). A plausible mechanism for Pb(II) adsorption could be the electrostatic interaction of the metal cation with the −OH and possibly −COOH groups on the surface of the nanoadsorbents.

3.2.2. Effect of Adsorbent Dose. The influence of the adsorbent concentration was examined by varying the amount of composite and the original Fe_3O_4 NPs from 0.03 to 0.15 g with the pH of the solution 8, contact time of 80 min, Pb(II) ion concentration of 60 mg/L, and at 25 °C with agitation speed 200 rpm. As displayed in Figure 7a,b, when increasing

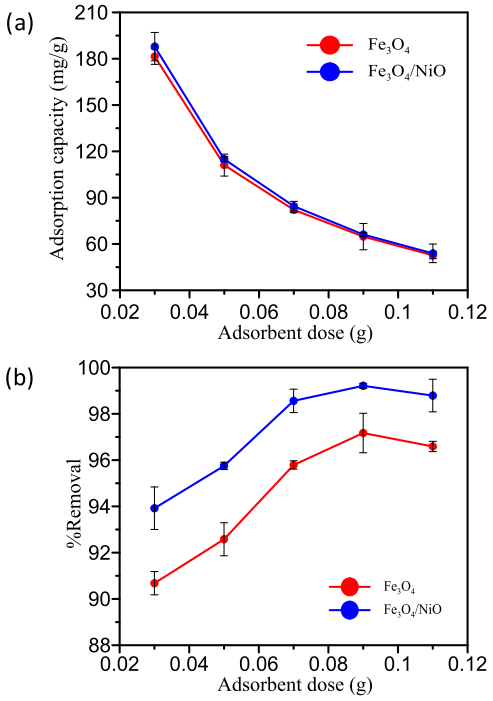

Figure 7. Effect of adsorbent dosage on the (a) adsorption capacity of Pb and (b) removal efficiency of Pb Fe_3O_4 and 50% Fe_3O_4/NiO nanocomposite.

the amount of adsorbent dose, the removal efficiency increased up to 0.09 g; this amount of dose was the optimum condition, which then slightly decreased beyond the optimum dosage. The adsorption capacities for both were observed to be maximum at the lower adsorbent amount and decreased as the dose increased. Fe_3O_4 NPs and the Fe_3O_4/NiO nanocomposite showed almost nearly the same response in this study. The decreased adsorption capacity was observed as the adsorbent dose increased, which was accredited to adsorption sites remaining unsaturated throughout the adsorption reaction on account of the higher number of accessible adsorption sites favoring improved Pb ion uptake.[38] The availability of a larger surface area and adsorption sites for a constant number of Pb ions increased the adsorption dosage.[39] The maximum removal efficiency at 0.09 g was 97.17% for Fe_3O_4 NPs and 99.21% for Fe_3O_4/NiO(1:1) (Figure 7b).

3.2.3. Effect of Initial Pb Ion Concentration and Contact Time. The initial concentration of the adsorbate is one of the most vital factors influencing the adsorption process. The effect of Pb ion concentration was determined by adding 60, 80, 100, 120, and 140 mg/L concentrations of Pb (II) in a 60 mL sample size in a 100 mL Erlenmeyer flask. The optimum dose of 0.09 g for Fe_3O_4 and 50% Fe_3O_4/NiO was added to each of the above Pb ion concentrations at pH 8, and it was stirred for 80 min. The adsorption ability and elimination efficiency of this study are displayed in Figure 8a,b. The maximum percent removal efficiencies of Fe_3O_4 and Fe_3O_4/NiO nanoadsorbents were calculated to be 86.07 and 98.11%, respectively, at 100

https://doi.org/10.1021/acsomega.3c08151
ACS Omega 2024, 9, 6803−6814

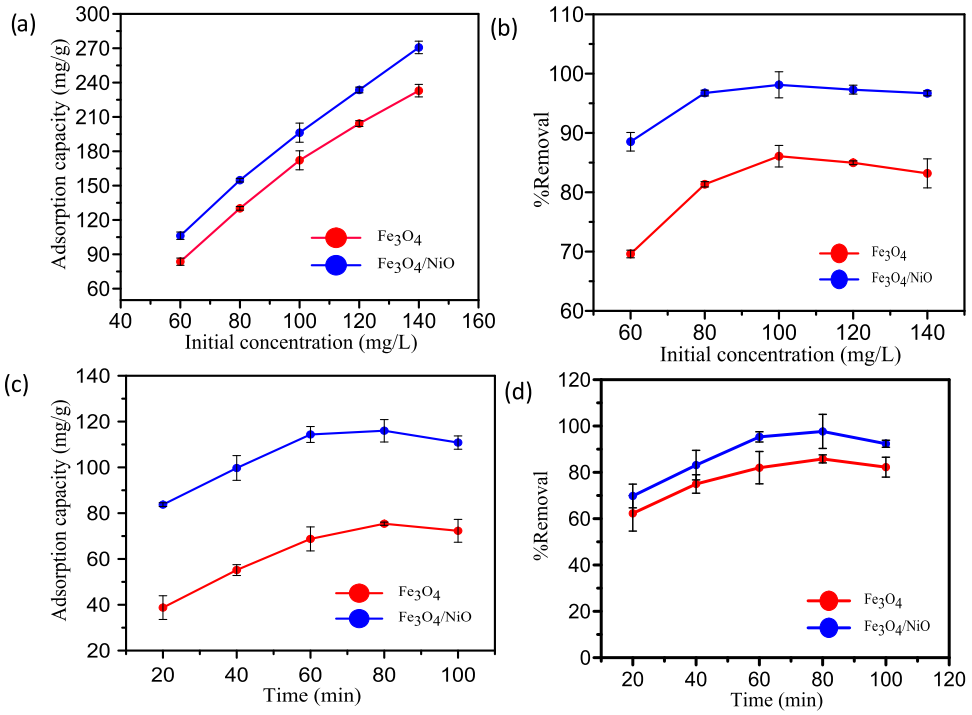

Figure 8. Effect of (a) initial Pb concentration on adsorption capacity, (b) initial Pb concentration on removal efficiency, (c) adsorption time on adsorption capacity, and (d) adsorption time on removal efficiency of Pb by Fe_3O_4 and the 50% Fe_3O_4/NiO nanocomposite.

Table 1. Comparison of the Pb(II) Adsorption Capacity and %Removal Efficiency of the Fe_3O_4/NiO Nanocomposite with the Reported Adsorbents

adsorbent	capacity (mg g^{-1})	Pb(II) %removal efficiency (%)	adsorption time (min)	reference
Fe_3O_4/NiO	123.74	97.65	80	this work
waste sugar cane bagasse	1.61	89.31	90	41
lignin-based magnetic	L1@MNP = 111.23 L2@MNP = 81.97	85	30	42
ZnOnp-CSD matrix	92.59	81.96	100	43
PH-*g*-MMA-without catalyst	with cat. 370.40 without cat. 137.0	99.30	63.75	44
magnetic MOF composite	219	90		45

mg/L Pb concentration. With a further increase in adsorbate concentration, a slight decrease in the removal efficiency was observed. The acceleration of Pb ion diffusion into the adsorbents caused by an increase in concentration gradient with increasing Pb concentration could explain the increased adsorption capacity and removal efficiency.[40] As a result, the extent of Pb uptake by adsorbents increases significantly with an increasing contact time. The removal efficiency of the Pb ion by Fe_3O_4 and Fe_3O_4/NiO was studied at various intervals (20−120 min) using optimum pH, Pb concentration, and adsorbent dosage (Figure 8c,d). As the adsorption time increased, both the removal efficiency and the adsorption capacity increased until they reached equilibrium. The optimum contact time was 80 min, with removal efficiencies of 85.8% and 97.65% for Fe_3O_4 and Fe_3O_4/NiO, respectively. Adsorption studies revealed that the removal efficiency and adsorption capacity of Pb by Fe_3O_4/NiO were significantly higher than those of Fe_3O_4 NPs.

After evaluating the efficiency of the prepared nanocomposite for lead ion removal from wastewater, we compared its performance with other adsorbents reported to be useful for a similar application. The comparison showing the %removal efficiency of different materials is summarized in Table 1. With a more significant percentage of removal, because our nanoadsorbent is affordable, user-friendly, environmentally friendly, and quick to remove heavy metal ions from vast volumes of wastewater using an external magnetic field, it meets the requirements for better removal efficiencies and its most effective wastewater treatment methods, which is a problem in other adsorbent materials. Fe_3O_4 NPs alone have poorer removal efficiencies, though. When NiO NPs are added to a composite, they perform better and can be extracted from vast volumes of water by using an external magnet. In general, the Fe_3O_4/NiO nanocomposite showed highly efficient lead ion removal, which is better than some of the reported adsorbents.

3.3. Adsorption Isotherms. To understand the nature of the adsorption process, we have studied the most common adsorption processes through the most common isotherm models: Langmuir and Freundlich isotherms. In the case of the Langmuir isotherm, the adsorption process takes place at monolayer, homogeneous locations. Mathematically, it can be given by the following equation.[46]

https://doi.org/10.1021/acsomega.3c08151
ACS Omega 2024, 9, 6803−6814

$$\frac{c_e}{q_e} = \frac{1}{K_L q_m} + \frac{c_e}{q_m} \quad (4)$$

where q_m is the maximum monolayer adsorption capacity (mg/g); K_L is the Langmuir constant, which is associated with the energy of adsorption (L/g); and q_e and c_e are the adsorption capacity (mg/g) and equilibrium concentration (mg/L), respectively. Plotting $\frac{c_e}{q_e}$ vs c_e from the above equation results in a straight line of slope $\frac{1}{q_m}$ and intercepts $\frac{1}{K_L q_m}$. The R_L values decide the favorability of the adsorption isotherm, as unfavorable ($R_L > 1$), linear ($R_L = 1$), favorable ($0 < R_L < 1$), or irreversible ($R_L = 0$).

$$R_L = \frac{1}{1 + K_L C_0} \quad (5)$$

where C_0 is the initial concentration of the metal ion.

The Freundlich adsorption isotherm is used for multilayer adsorption and heterogeneous surfaces, and it can be given by the following equation.[47]

$$\log q_e = \log K_f + \frac{1}{n} \log c_e \quad (6)$$

where K_f indicates the Freundlich isotherm capacity (mg/g) and n represents the adsorption intensity. A straight line with a slope K_f and intercept $1/n$ is obtained by plotting ln q_e vs ln c_e. The value of n determines whether the adsorption is physical or chemical. The results obtained from the isotherm models, the constants, and correlation coefficients (R^2) are presented in Table 2. The R_L value (separation factor) of the Langmuir

Table 2. Isotherm Models for Pb(II) Ion Removal Using a Magnetic Nanoadsorbent (Fe_3O_4/NiO)

types of isotherm	parameters	adsorbate/Pb(II)
Langmuir	Q_{max} (mg g^{-1})	751.88
	K_L (L mg^{-1})	101.95
	R_L	1.02
	R^2	0.8653
Freundlich	K_f ((mg·g^{-1})(L$^{1/n}$·$mg^{-1/n}$))	3.9994
	$1/n$	0.8425
	R^2	0.9524

model shows the feasibility of the adsorption mechanism.[48] In this work, the values of R_L were ($R_L > 1$) at various adsorbate dosages, and these endorse that there is unfavorable adsorption.[49] Results displayed that (Table 2) the higher R^2 value of the Freundlich model suggested that the Freundlich isotherm was best fitting compared to the Langmuir isotherm, indicating that the adsorbent surface is heterogeneous. In this study, the parameter n is greater than unity in the Freundlich isotherm, confirming that the adsorption of the Pb ion onto the Fe_3O_4/NiO nanocomposite is a favorable and chemical interaction.[50]

3.4. Adsorption Kinetics. The pseudo-first-order and pseudo-second-order kinetic models investigated the kinetics of the Pb adsorption process. Pseudo-first-order kinetics depends on the weak interaction between the adsorbate and adsorbent, specifically governing physical adsorption. In contrast, the pseudo-second-order kinetic model governs the chemical interaction adsorption process.[51,52] To analyze the kinetics, pseudo-first-order and second-order kinetic equations were applied.

$$\log(q_e - q_t) = \log q_e - k_1/2.303t \quad (7)$$

$$t/q_t = 1/k_2 q^2 e + 1/q_e t \quad (8)$$

Here, q_t and q_e are Pb ion adsorption capability at contact time (t) and equilibrium in mg/g, respectively, and k_1 (min^{-1}) and k_2 (g/mg/min) are the pseudo-first-order and pseudo-second-order rate constants, respectively. Table 3 displays the values of

Table 3. Parameter of the Kinetic Models for the Adsorption of the Pb(II) Ion Using Fe_3O_4/NiO

kinetic models	parameters	adsorbate/Pb(II)
pseudo-first-order	q_e exe (mg g^{-1})	123.74
	q_e cal (mg g^{-1})	67.79
	k_1 (min^{-1})	0.000034
	R^2	0.50
pseudo-second-order	q_e exe (mg g^{-1})	123.74
	q_e cal (mg g^{-1})	123.46
	k_2 (g/mg·min^{-1})	228852.5
	R^2	0.9914

the k_1 and k_2 constants and adsorption equilibrium q_e for the pseudo-first order and second order for the Fe_3O_4/NiO nanocomposite adsorbent. The coefficient (R^2) value was calculated to be higher for the pseudo-second-order (R^2 = 0.9914) and lower for the pseudo-first-order (R^2 = 0.50). Consequently, the adsorption kinetic mechanism was governed by pseudo-second-order kinetics, which agrees with adsorption isotherm studies.

3.5. Recovery Studies. In many applications, reuse of the adsorbent via the regeneration of its adsorption properties is an economic necessity. With rising prices of raw materials and wastewater treatment processes, the attractiveness of product recovery processes has increased significantly. The magnetic nanocomposite adsorbent could be easily and readily separated from the reaction mixture. The recycling results displayed in Table 4 were found to have retained their activity despite

Table 4. Recycling of Magnetic Nanocomposites (Fe_3O_4/NiO: 50%) as an Adsorbent

cycles	1st	2nd	3rd
%removal	97.24%	94.12%	89.56%

showing a decrease in the removal efficiency of Pb(II), and it depends on the pH of a solution and was performed by adding HCl and NaOH to solution.

The reusability of the nanoadsorbents was conducted according to the reported literature procedure with some modifications.[53] In a typical experiment, the recycling test was performed by adding 0.01 M HNO_3 or HCl and 0.005 M NaOH eluent to the solution. Initially, metals were adsorbed on the nanoadsorbent from 60 mL solutions containing 100 mg/L metal ions at a pH of 8. Then, nanoadsorbents were stripped using 30 mL of eluent by agitating at 25 °C for 30 min. The nanoadsorbents were separated, and the supernatant's metal ion concentration was analyzed. For each measurement, the adsorption−desorption cycles were repeated three times.

https://doi.org/10.1021/acsomega.3c08151
ACS Omega 2024, 9, 6803−6814

The findings indicate that Fe_3O_4/NiO magnetic nanocomposites have good stability and reusability as studied up to 3 cycles.

4. CONCLUSIONS

Fe_3O_4, NiO, and Fe_3O_4/NiO were fruitfully synthesized using *H. abyssinica* leaf extract as a capping and reducing agent via a greener coprecipitation method. The crystallite, morphology, functional groups, and surface area were studied by XRD, SEM, FT-IR, and N_2 adsorption at the cryogenic condition, respectively. Results showed that the introduction of 50%NiO increased the surface area of the composite compared with Fe_3O_4 NPs while retaining the magnetic properties of Fe_3O_4. Fe_3O_4 and 50%Fe_3O_4/NiO nanocomposite were tested for their adsorption performances toward Pb(II) and gave 85.8 and 97.65% removal efficiencies, respectively. Adding optimum amounts of Ni in the preparation of Fe_3O_4/NiO composites with the *H. abyssinica* plant extract enhances the adsorption efficiency. More importantly, the adsorption kinetic mechanism was governed by pseudo-second-order kinetics, which is in good agreement with adsorption isotherm studies, which is a Freundlich isotherm, confirming that the adsorption of the Pb ion onto the Fe_3O_4/NiO nanocomposite is a chemical interaction. The reusability of the magnetic nanoadsorbent was performed by three cycles, and it shows elimination efficiency.

AUTHOR INFORMATION

Corresponding Author

Wubshet Mekonnen Girma − *Department of Chemistry, College of Natural Science, Wollo University, P.O. Box 1145 Dessie, Ethiopia;* orcid.org/0000-0003-3370-6731; Phone: +251-910804026; Email: wubshet.mekonnen@wu.edu.et

Authors

Abdurohman Eshetu Ferenj − *Department of Chemistry, College of Natural Science, Wollo University, P.O. Box 1145 Dessie, Ethiopia*

Daniel Manaye Kabtamu − *Department of Materials Science and Engineering, National Taiwan University of Science and Technology, Taipei 10607, Taiwan*

Ayalew H. Assen − *Department of Chemistry, College of Natural Science, Wollo University, P.O. Box 1145 Dessie, Ethiopia; Applied Chemistry and Engineering Research Centre of Excellence (ACER CoE), Mohammed VI Polytechnic University (UM6P), 43150 Ben Guerir, Morocco*

Gangaraju Gedda − *Central Research Laboratory, K S Hegde Medical Academy, NITTE (Deemed to be University), Mangaluru 575018 Karnataka, India; Department of Animal Science & Technology and BET Research Institute, Chung-Ang University, Anseong 17546 Gyeonggi-do, Republic of Korea*

Adem Ali Muhabie − *Department of Chemistry, Faculty of Natural and Computational Science, Woldia University, P.O. Box 400 Woldia, Ethiopia;* orcid.org/0000-0003-4609-5589

Mhamed Berrada − *Institute of Science Technology and Innovation (IST&I), Mohammed VI Polytechnic University, 43150 Ben Guerir, Morocco*

Complete contact information is available at: https://pubs.acs.org/10.1021/acsomega.3c08151

Notes

The authors declare no competing financial interest.

ACKNOWLEDGMENTS

The authors would like to thank Wollo University for funding. The authors also would like to gratefully acknowledge the National Taiwan Science and Technology University for SEM imaging, Adama Science and Technology University for XRD analysis, and Mohammed VI Polytechnic University (UM6P) of Morocco for N_2 sorption and ζ-potential measurements.

REFERENCES

(1) Almomani, F.; Bhosale, R.; Khraisheh, M.; Kumar, A.; Almomani, T. Heavy metal ions removal from industrial wastewater using magnetic nanoparticles (MNP). *Appl. Surf. Sci.* **2020**, *506*, No. 144924.

(2) Hu, J.; Chen, G.; Lo, I. M. Selective removal of heavy metals from industrial wastewater using maghemite nanoparticle: performance and mechanisms. *J. Environ. Eng.* **2006**, *132* (7), 709−715.

(3) Sun, Q.; Wang, W.; Yang, L.; Huang, S.; Xu, Z.; Ji, Z.; Li, Y.; Hu, Y. Separation and recovery of heavy metals from concentrated smelting wastewater by synergistic solvent extraction using a mixture of 2-hydroxy-5-nonylacetophenone oxime and bis (2, 4, 4-trimethylpentyl)-phosphinic acid. *Solvent Extr. Ion Exch.* **2018**, *36* (2), 175−190.

(4) Zhang, Y.; Duan, X. Chemical precipitation of heavy metals from wastewater by using the synthetical magnesium hydroxy carbonate. *Water Sci. Technol.* **2020**, *81* (6), 1130−1136.

(5) Ibrahim, Y.; Abdulkarem, E.; Naddeo, V.; Banat, F.; Hasan, S. W. Synthesis of super hydrophilic cellulose-alpha zirconium phosphate ion exchange membrane via surface coating for the removal of heavy metals from wastewater. *Sci. Total Environ.* **2019**, *690*, 167−180.

(6) Wang, Y.; Wang, B.; Wang, Q.; Di, J.; Miao, S.; Yu, J. Amino-functionalized porous nanofibrous membranes for simultaneous removal of oil and heavy-metal ions from wastewater. *ACS Appl. Mater. Interfaces* **2019**, *11* (1), 1672−1679.

(7) Azimi, A.; Azari, A.; Rezakazemi, M.; Ansarpour, M. Removal of heavy metals from industrial wastewaters: a review. *ChemBioEng Rev.* **2017**, *4* (1), 37−59.

(8) Shrestha, R.; Ban, S.; Devkota, S.; Sharma, S.; Joshi, R.; Tiwari, A. P.; Kim, H. Y.; Joshi, M. K. Technological trends in heavy metals removal from industrial wastewater: A review. *J. Environ. Chem. Eng.* **2021**, *9* (4), No. 105688.

(9) Huang, S.-H.; Chen, D.-H. Rapid removal of heavy metal cations and anions from aqueous solutions by an amino-functionalized magnetic nano-adsorbent. *J. Hazard. Mater.* **2009**, *163* (1), 174−179.

(10) Khulbe, K. C.; Matsuura, T. Removal of heavy metals and pollutants by membrane adsorption techniques. *Appl. Water Sci.* **2018**, *8* (1), 19.

(11) Mandal, S.; Calderon, J.; Marpu, S. B.; Omary, M. A.; Shi, S. Q. Mesoporous activated carbon as a green adsorbent for the removal of heavy metals and Congo red: Characterization, adsorption kinetics, and isotherm studies. *J. Contam. Hydrol.* **2021**, *243*, No. 103869.

(12) Khan, F. S. A.; Mubarak, N. M.; Tan, Y. H.; Khalid, M.; Karri, R. R.; Walvekar, R.; Abdullah, E. C.; Nizamuddin, S.; Mazari, S. A. A comprehensive review on magnetic carbon nanotubes and carbon nanotube-based buckypaper for removal of heavy metals and dyes. *J. Hazard. Mater.* **2021**, *413*, No. 125375.

(13) Gendy, E. A.; Ifthikar, J.; Ali, J.; Oyekunle, D. T.; Elkhlifia, Z.; Shahib, I. I.; Khodair, A. I.; Chen, Z. Removal of heavy metals by covalent organic frameworks (COFs): A review on its mechanism and adsorption properties. *J. Environ. Chem. Eng.* **2021**, *9* (4), No. 105687.

(14) Gil, A.; Santamaría, L.; Korili, S.; Vicente, M.; Barbosa, L.; de Souza, S.; Marçal, L.; De Faria, E.; Ciuffi, K. A review of organic-inorganic hybrid clay based adsorbents for contaminants removal: Synthesis, perspectives and applications. *J. Environ. Chem. Eng.* **2021**, *9* (5), No. 105808.

(15) Cho, S.; Kim, J.-H.; Yang, K. S.; Chang, M. Facile preparation of amino-functionalized polymeric microcapsules as efficient adsorbent for heavy metal ions removal. *Chem. Eng. J.* **2021**, *425*, No. 130645.
(16) Hassen, Y. E.; Gedda, G.; Assen, A. H.; Kabtamu, D. M.; Girma, W. M. Dodonaea angustifolia Extract-Assisted Green Synthesis of the Cu2O/Al2O3 Nanocomposite for Adsorption of Cd (II) from Water. *ACS Omega* **2023**, *8* (19), 17209−17219.
(17) Mahmoud, M. E.; Abdelwahab, M. S.; Fathallah, E. M. Design of novel nano-sorbents based on nano-magnetic iron oxide−bound-nano-silicon oxide−immobilized-triethylenetetramine for implementation in water treatment of heavy metals. *Chem. Eng. J.* **2013**, *223*, 318−327.
(18) Kalantari, S.; Yousefpour, M.; Taherian, Z. Synthesis of mesoporous silica/iron oxide nanocomposites and application of optimum sample as adsorbent in removal of heavy metals. *Rare Met.* **2017**, *36* (12), 942−950.
(19) Sun, Y.-t.; Chen, J.-d.; Wei, Z.-h.; Chen, Y.-k.; Shao, C.-l.; Zhou, J.-f. Copper ion removal from aqueous media using banana peel biochar/Fe3O4/branched polyethyleneimine. *Colloids Surf., A* **2023**, *658*, No. 130736.
(20) Krishna Kumar, A. S.; Jiang, S.-J.; Warchoł, J. K. Synthesis and characterization of two-dimensional transition metal dichalcogenide magnetic MoS2@ Fe3O4 nanoparticles for adsorption of Cr (VI)/Cr (III). *ACS Omega* **2017**, *2* (9), 6187−6200.
(21) Liu, Y.; Luo, C.; Cui, G.; Yan, S. Synthesis of manganese dioxide/iron oxide/graphene oxide magnetic nanocomposites for hexavalent chromium removal. *RSC Adv.* **2015**, *5* (67), 54156−54164.
(22) Zhu, Q.; Tao, F.; Pan, Q. Fast and selective removal of oils from water surface via highly hydrophobic core− shell Fe2O3@ C nanoparticles under magnetic field. *ACS Appl. Mater. Interfaces* **2010**, *2* (11), 3141−3146.
(23) Chu, Y.; Pan, Q. Three-dimensionally macroporous Fe/C nanocomposites as highly selective oil-absorption materials. *ACS Appl. Mater. Interfaces* **2012**, *4* (5), 2420−2425.
(24) Calcagnile, P.; Fragouli, D.; Bayer, I. S.; Anyfantis, G. C.; Martiradonna, L.; Cozzoli, P. D.; Cingolani, R.; Athanassiou, A. Magnetically driven floating foams for the removal of oil contaminants from water. *ACS Nano* **2012**, *6* (6), 5413−5419.
(25) Banerjee, A.; Gokhale, R.; Bhatnagar, S.; Jog, J.; Bhardwaj, M.; Lefez, B.; Hannoyer, B.; Ogale, S. MOF derived porous carbon−Fe 3 O 4 nanocomposite as a high performance, recyclable environmental superadsorbent. *J. Mater. Chem.* **2012**, *22* (37), 19694−19699.
(26) Wang, G.; Sun, Q.; Zhang, Y.; Fan, J.; Ma, L. Sorption and regeneration of magnetic exfoliated graphite as a new sorbent for oil pollution. *Desalination* **2010**, *263* (1−3), 183−188.
(27) Venkatanarasimhan, S.; Raghavachari, D. Epoxidized natural rubber−magnetite nanocomposites for oil spill recovery. *J. Mater. Chem. A* **2013**, *1* (3), 868−876.
(28) Tempesti, P.; Bonini, M.; Ridi, F.; Baglioni, P. Magnetic polystyrene nanocomposites for the separation of oil and water. *J. Mater. Chem. A* **2014**, *2* (6), 1980−1984.
(29) Xu, C.; Yang, W.; Liu, W.; Sun, H.; Jiao, C.; Lin, A.-j. Performance and mechanism of Cr (VI) removal by zero-valent iron loaded onto expanded graphite. *J. Environ. Sci.* **2018**, *67*, 14−22.
(30) Aisida, S. O.; Ugwu, K.; Nwanya, A. C.; Bashir, A.; Nwankwo, N. U.; Ahmed, I.; Ezema, F. I. Biosynthesis of silver oxide nanoparticles using leave extract of Telfairia Occidentalis and its antibacterial activity. *Mater. Today: Proc.* **2021**, *36*, 208−213, DOI: 10.1016/j.matpr.2020.03.005.
(31) Melkamu, W. W.; Bitew, L. T. Green synthesis of silver nanoparticles using Hagenia abyssinica (Bruce) JF Gmel plant leaf extract and their antibacterial and anti-oxidant activities. *Heliyon* **2021**, *7* (11), No. e08459.
(32) Wolde, T.; Bizuayehu, B.; Hailemariam, T.; Tiruha, K. Phytochemical analysis and antimicrobial activity of Hagenia abyssinica. *Indian J. Pharm. Pharmacol.* **2016**, *3* (3), 127−134.
(33) Venkateswarlu, S.; Yoon, M.; Kim, M. J. An environmentally benign synthesis of Fe3O4 nanoparticles to Fe3O4 nanoclusters: Rapid separation and removal of Hg (II) from an aqueous medium. *Chemosphere* **2022**, *286*, No. 131673.
(34) Molnár, Z.; Bódai, V.; Szakacs, G.; Erdélyi, B.; Fogarassy, Z.; Sáfrán, G.; Varga, T.; Kónya, Z.; Tóth-Szeles, E.; Szűcs, R.; Lagzi, I. Green synthesis of gold nanoparticles by thermophilic filamentous fungi. *Sci. Rep.* **2018**, *8* (1), No. 3943.
(35) Masuku, M.; Ouma, L.; Pholosi, A. Microwave assisted synthesis of oleic acid modified magnetite nanoparticles for benzene adsorption. *Environ. Nanotechnol. Monit. Manage.* **2021**, *15*, No. 100429.
(36) Zhang, M.; Wang, W.; Cui, Y.; Chu, X.; Sun, B.; Zhou, N.; Shen, J. Magnetofluorescent Fe3O4/carbon quantum dots coated single-walled carbon nanotubes as dual-modal targeted imaging and chemo/photodynamic/photothermal triple-modal therapeutic agents. *Chem. Eng. J.* **2018**, *338*, 526−538.
(37) Karami, H. Heavy metal removal from water by magnetite nanorods. *Chem. Eng. J.* **2013**, *219*, 209−216.
(38) Sarojini, G.; Venkateshbabu, S.; Rajasimman, M. Facile synthesis and characterization of polypyrrole-iron oxide−seaweed (PPy-Fe3O4-SW) nanocomposite and its exploration for adsorptive removal of Pb (II) from heavy metal bearing water. *Chemosphere* **2021**, *278*, No. 130400.
(39) Rani, M.; Yadav, J.; Shanker, U. Green synthesis, kinetics and photoactivity of novel nickel oxide-decorated zinc hexacyanocobaltate catalyst for efficient removal of toxic Cr (VI). *J. Environ. Chem. Eng.* **2021**, *9* (2), No. 105073.
(40) Xin, X.; Wei, Q.; Yang, J.; Yan, L.; Feng, R.; Chen, G.; Du, B.; Li, H. Highly efficient removal of heavy metal ions by amine-functionalized mesoporous Fe3O4 nanoparticles. *Chem. Eng. J.* **2012**, *184*, 132−140.
(41) Ezeonuegbu, B. A.; Machido, D. A.; Whong, C. M.; Japhet, W. S.; Alexiou, A.; Elazab, S. T.; Qusty, N.; Yaro, C. A.; Batiha, G. E.-S. Agricultural waste of sugarcane bagasse as efficient adsorbent for lead and nickel removal from untreated wastewater: Biosorption, equilibrium isotherms, kinetics and desorption studies. *Biotechnol. Rep.* **2021**, *30*, No. e00614.
(42) Zhou, X.; Jin, C.; Liu, G.; Wu, G.; Huo, S.; Kong, Z. Functionalized lignin-based magnetic adsorbents with tunable structure for the efficient and selective removal of Pb (II) from aqueous solution. *Chem. Eng. J.* **2021**, *420*, 130409−130418.
(43) Aigbe, R.; Kavaz, D. Unravel the potential of zinc oxide nanoparticle-carbonized sawdust matrix for removal of lead (II) ions from aqueous solution. *Chin. J. Chem. Eng.* **2021**, *29*, 92−102.
(44) Chaduka, M.; Guyo, U.; Zinyama, N. P.; Tshuma, P.; Matsinha, L. C. Modeling and optimization of lead (II) adsorption by a novel peanut hull-g-methyl methacrylate biopolymer using response surface methodology (RSM). *Anal. Lett.* **2020**, *53* (8), 1294−1311.
(45) Shi, Z.; Xu, C.; Guan, H.; Li, L.; Fan, L.; Wang, Y.; Liu, L.; Meng, Q.; Zhang, R. Magnetic metal organic frameworks (MOFs) composite for removal of lead and malachite green in wastewater. *Colloids Surf., A* **2018**, *539*, 382−390.
(46) Langmuir, I. The adsorption of gases on plane surfaces of glass, mica and platinum. *J. Am. Chem. Soc.* **1918**, *40* (9), 1361−1403.
(47) Freundlich, H. M. F. Over the adsorption in solution. *J. Phys. Chem. A* **1906**, *57*, 385−471.
(48) Vishali, S.; Mullai, P. Analysis of two-parameter and three-parameter isotherms by nonlinear regression for the treatment of textile effluent using immobilized Trametes versicolor: comparison of various error functions. *Desalin. Water Treat.* **2016**, *57* (56), 27061−27072.
(49) Khalith, S. B. M.; Anirud, R. R.; Ramalingam, R.; Karuppannan, S. K.; Dowlath, M. J. H.; Pandion, K.; Ravindran, B.; Woong Chang, S.; Ovi, D.; Arasu, M. V.; et al. Synthesis and characterization of magnetite carbon nanocomposite from agro waste as chromium adsorbent for effluent treatment. *Environ. Res.* **2021**, *202*, No. 111669, DOI: 10.1016/j.envres.2021.111669.
(50) Reed, B. E.; Matsumoto, M. R. Modeling cadmium adsorption by activated carbon using the Langmuir and Freundlich isotherm expressions. *Sep. Sci. Technol.* **1993**, *28* (13−14), 2179−2195.

(51) Qiu, H.; Lv, L.; Pan, B.-c.; Zhang, Q.-j.; Zhang, W.-m.; Zhang, Q.-x. Critical review in adsorption kinetic models. *J. Zhejiang Univ.-Sci. A* **2009**, *10* (5), 716−724.
(52) Ho, Y.-S.; McKay, G. Pseudo-second order model for sorption processes. *Process Biochem.* **1999**, *34* (5), 451−465.
(53) Rajput, S.; Pittman, C. U., Jr.; Mohan, D. Magnetic magnetite (Fe3O4) nanoparticle synthesis and applications for lead (Pb2+) and chromium (Cr6+) removal from water. *J. Colloid Interface Sci.* **2016**, *468*, 334−346.

https://doi.org/10.1021/acsomega.3c08151
ACS Omega 2024, 9, 6803−6814